*17th World Conference on Earthquake Engineering, 17WCEE*
*Sendai, Japan - September 13th to 18th 2020*

# DYNAMIC CHARACTERISTICS OF PILE TOP SEISMIC ISOLATION BUILDINGS CONSIDERING VARIABLE AXIAL LOAD

T. Yamauchi[1], H. Kitamura[2], M. Nagano[3], T. Sato[4], K. Suzuki[5], Y. Matsuda[6], Y. Tobita[7]

[1] *Technical Research Institute, Asanuma Corporation, yamauchi-toyohide@asanuma.co.jp*
[2] *Vice-President, Tokyo University of Science, kita-h@rs.noda.tus.ac.jp*
[3] *Professor, Tokyo University of Science, nagano-m@rs.noda.tus.ac.jp*
[4] *Associate Professor, Kyushu University, sato@arch.kyushu-u.ac.jp*
[5] *Researcher, Forestry and Forest Products Research Institute, suzukik777@ffpri.affrc.go.jp*
[6] *Assistant Professor, Tokyo University of Science, matsuda_y@rs.tus.ac.jp*
[7] *Technical Research Institute, Asanuma Corporation, tobita-yoshinori@asanuma.co.jp*

## *Abstract*

A pile top seismic isolation system is used for constructing base-isolated buildings. In this system, seismic isolators are directly set on top of the pile. The piles are connected by thin foundation girders or a mat slab. In recent years, many logistics centers in Japan have been constructed using this system because it enables significant cost reductions in underground construction. However, there are known disadvantages associated with this system, which require a more sophisticated treatment of horizontal and rotational stiffnesses of a laminated rubber bearing.

We performed numerical experiments via earthquake response analyses for a pile top seismic isolation building; this was carried out using an analytical model of a laminated rubber bearing based on Haringx's theory. This model considers the effects of bending and rotational deformation at the laminated rubber bearing's bottom part. In addition, we proposed a set of methods to evaluate the dynamic mechanical characteristics of laminated rubber bearings and apply a seismic deformation method for piles. In the present study, we explored these proposed methods' applicability to the outer part of a building, considering a variable axial load acting on the laminated rubber bearing. This follows from previous studies, where the axial load of the analytical model was kept constant.

In this paper, we describe the results of our evaluation of the dynamic characteristics of laminated rubber bearings and piles on the outer part of a pile top seismic isolation building using a two-dimensional elasto-plastic frame model. The frame model represents a logistics center and consists of a superstructure with 4 stories and 10 spans, a seismic isolated layer, thin foundation girders, 11 piles, free field, and soil–pile springs that connect the piles and the free field.

The following conclusions are drawn:

1. The dynamic mechanical characteristics of laminated rubber bearings can be evaluated by adapting the proposed method considering the variable axial loads.
2. The bending moment distribution of piles located on the outer part of a building is quantitatively evaluated, and the effects of variable axial load are clarified. In addition, the seismic deformation method used in a previous study can be applied to piles located on the outer part of a building.

*Keywords: Pile Top Seismic Isolation System, Variable Axial Load, Dynamic Characteristic*

 



## 1. Introduction

In seismic engineering, a pile top seismic isolation system is used for constructing base-isolated buildings. In this system, seismic isolators are directly set on the top of the pile and the piles are connected to thin foundation girders or a mat slab. In recent years, many logistics centers in Japan have been constructed using this system because it enables significant cost reductions in underground construction.

However, this system has disadvantages. For example, the bottom part of the laminated rubber bearing on the thin foundation girders easily undergoes bending rotation because of the girder's low stiffness. If bending rotation occurs, the laminated rubber bearing's horizontal stiffness reduces due to the horizontal component of axial load, and its inflection point is moved downward from the center height of the device (usually, this point should not move) [1, 2]. This, in turn, significantly affects the structural characteristics of the pile top seismic isolation building.

In previous studies, we performed earthquake response analyses for a pile top seismic isolation building [3-5]. In addition, we proposed a set of methods that evaluates the dynamic mechanical characteristics of the laminated rubber bearing and applies a seismic deformation method for piles [3-5]. In the present study, we retain our focus on the applicability of these methods to the outer part of a building, where we now consider a variable axial load acting on a laminated rubber bearing, in contrast with the constant axial load considered in previous studies [3-5].

This paper describes the results of our evaluation of the dynamic characteristics of laminated rubber bearings and piles located on the outer part in a pile top seismic isolation building by earthquake response analyses using a two-dimensional elasto-plastic frame model.

## 2. Outline of Dynamic Analysis

### 2.1 Analytical Model of Pile Top Seismic Isolation Building

Figure 1 shows the dynamic analytical model. The analytical model is a two-dimensional frame model, and it represents one surface of the pile top seismic isolation building. It consists of a superstructure with 4 stories and 10 spans, a seismic isolated layer, thin foundation girders, 11 piles, soil–pile springs, and a free field.

The superstructure model comprises a mixed structure (RC columns and steel girders). All frames of the superstructure model are elastic beam elements. The compressive strength of concrete $f_c$ in the RC columns is 36 N/mm$^2$, and their Young's modulus is calculated from the compressive strength [6]. The Young's modulus of steel is 205,000 N/mm$^2$ [7]. The seismic isolated layer is constructed from a steel damper and a laminated rubber bearing. The steel damper has a normal bilinear model; its yield shear forces are 240.4 kN on the inner part and 120.2 kN on the outer part (Figure 1). The laminated rubber bearing is a natural rubber bearing; an overview of its parameters is shown in Table 1. The axial loads acting on the laminated rubber bearing are 8,000 kN (axial stress: 10.2 N/mm$^2$) on the inner part and 4,000 kN (axial stress: 10.4 N/mm$^2$) on the outer part. The laminated rubber bearing model will be described in detail in later sections. The primary equivalent natural period of the superstructure is approximately 3.2 s. The eigenvalue problem of the superstructure is detailed in a previous study [4].

The thin foundation girders and piles are used as parameters in the dynamic analyses because they influence the bending rotation of the laminated rubber bearing. The thin foundation girders have an RC structure. The model of the thin foundation girders contains elastic beam elements. Table 2 shows the section size of the thin foundation girder. Table 2 also shows the relative stiffness ratio of the thin foundation girder (FG/1G). There are two types of piles: steel and RC, that are of different cross-sectional shapes on their inner and outer parts (Table 2). The model for the piles contains elastic beam elements.

The free field and soil–pile springs are modeled according to "Soil-2" in [8]. Table 3 shows the profile of Soil-2. Table 4 shows the equivalent natural period of Soil-2. The stiffness of the soil–pile springs is calculated by Francis's equation [8] as in a previous report [4]. The soil–pile springs in the subsurface layers have a hyperbolic model. The ultimate strength of the subgrade reactions in the subsurface layers is calculated by Broms's equation [8]. The free field is a large lumped mass model with a cross-sectional area of 100,000m$^2$. The subsurface layers have an H–D model [9], and Figure 2 shows the strain dependency [10].



 



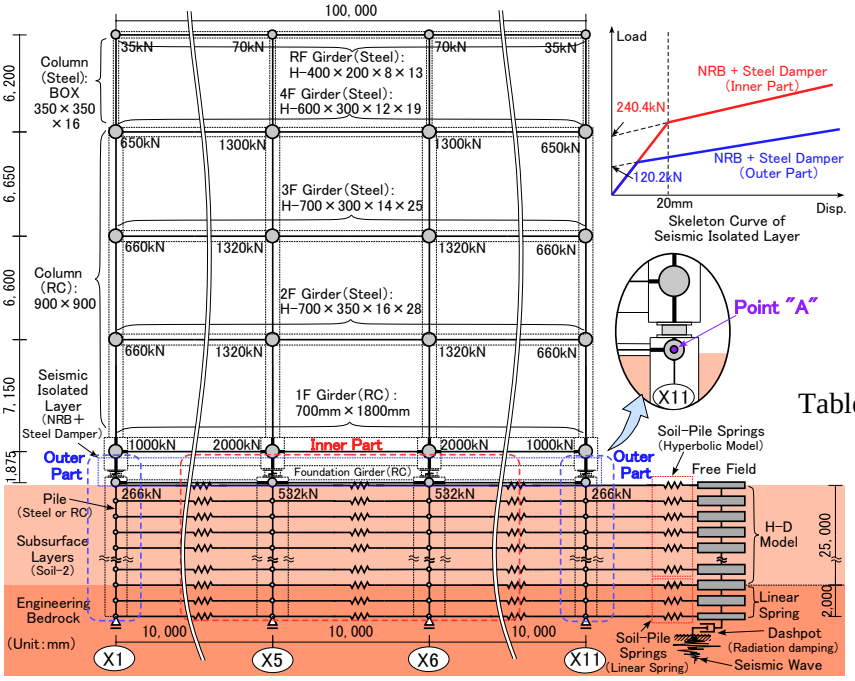


Fig.1 – Analytical model

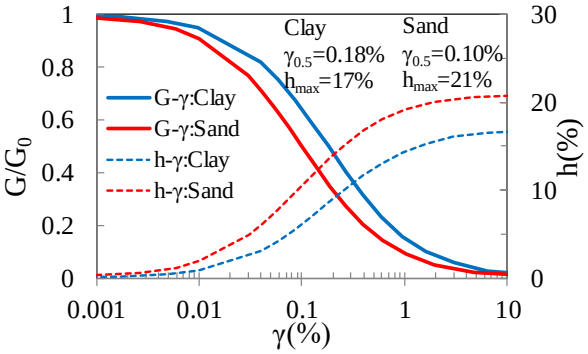


Fig.2 – Strain dependency of ground (G-$\gamma$ , h-$\gamma$ )

Table 1 – Overview of NRB

| Item | Inner part | Outer part |
|---|---|---|
| Shear modulus : $G$ (N/mm$^2$) | 0.39 | |
| Young's modulus : $E_0$(N/mm$^2$) | 1.17 | |
| Correction factor : $\kappa$ | 0.85 | |
| Bulk modulus : $E_\infty$(N/mm$^2$) | 1,961 | |
| Outer diameter : $D$ (mm) | 1,000 | 700 |
| Inner diameter : $d$ (mm) | 25 | 15 |
| Total rubber thickness : $n \cdot t_r$ (mm) | 200 | 140 |
| Primary shape factor : $S_1$ | 36.4 | |
| Secondary shape factor : $S_2$ | 5.0 | |
| Bending elastic modulus : $E_{rb}$ (N/mm$^2$) $E_{rb}=\frac{E_b \cdot E_\infty}{E_b+E_\infty}$, $\left(E_b=\left(1+\frac{2}{3}\kappa S_1^2\right)\right)$ | 606.8 | 608.1 |

Table 2 – Parameters of dynamic analysis

| Foundation girder (FG) | Pile | | |
|---|---|---|---|
| | Type | Inner part | Outer part |
| Pin joint (0.0) | Steel pile | Diameter : 1,200mm, t :19mm | Diameter : 800mm, t :14mm |
| B:1,000mm×D:350mm (0.011) | | | |
| B:2,000mm×D:350mm (0.021) | | | |
| B:3,000mm×D:350mm (0.032) | RC pile | Diameter : 2,000mm | Diameter : 1,400mm |
| B:4,000mm×D:350mm (0.042) | | | |
| RC structure: $f_c$=36N/mm$^2$ The numbers in paretheses are the relative stiffness ratio (FG/1G). | Steel pile : $E_s$=205,000N/mm$^2$ RC pile: $fc$=36N/mm$^2$ | | |

Table 3 – Profile of Soil-2 [8]

| Layer No | Depth (m) | Layer thickness (m) | Density ρ (t/m$^3$) | S-wave velocity $V_S$ (m/s) | P-wave velocity $V_P$ (m/s) | Type |
|---|---|---|---|---|---|---|
| 1 | 4.5 | 4.5 | 1.8 | 90 | 1,360 | Clay |
| 2 | 10.0 | 5.5 | 1.6 | 150 | 1,560 | Sand |
| 3 | 17.0 | 7.0 | 1.8 | 210 | 1,560 | Sand |
| 4 | 18.5 | 1.5 | 1.7 | 150 | 1,560 | Clay |
| 5 | 25.0 | 6.5 | 1.8 | 260 | 1,560 | Sand |
| Engineering Bedrock | - | - | 1.8 | 390 | 1,700 | - |

Table 4 – Equivalent natural period of Soil-2

| | 1st | 2nd | 3rd |
|---|---|---|---|
| Equivalent natural period (s) | 1.01 s | 0.38 s | 0.24 s |

## 2.2 Nonlinear Analytical Model of the Laminated Rubber Bearing

The analytical model of the laminated rubber bearing is based on Miyama's method [2], as in a previous study [4]. The definition of deformation of a laminated rubber bearing according to Miyama is shown in Figure 3. Miyama proposed a stiffness matrix for the laminated rubber bearing based on Haringx's theory [11]. The stiffness matrix is constructed using three matrices: the horizontal stiffness matrix [$K_H$], the geometric nonlinear matrix [$K_P$], and the rotational stiffness matrix [$K_R$] (Eq.(1)).

$$\begin{Bmatrix} Q_A \\ M_A \\ Q_B \\ M_B \end{Bmatrix} = \left[ [K_H] + [K_P] + [K_R] \right] \begin{Bmatrix} x_A \\ \theta_A \\ x_B \\ \theta_B \end{Bmatrix}$$

$$= \left[ K_h \begin{bmatrix} 1 & -h/2 & -1 & -h/2 \\ & h^2/4 & h/2 & h^2/4 \\ & & 1 & h/2 \\ & sym. & & h^2/4 \end{bmatrix} + P \begin{bmatrix} 1 & -1/2 & 0 & -1/2 \\ & h/4 & 1/2 & h/4 \\ & & 0 & 1/2 \\ & sym. & & h/4 \end{bmatrix} + K_r \begin{bmatrix} 0 & 0 & 0 & 0 \\ & 1 & 0 & -1 \\ & & 0 & 0 \\ & sym. & & 1 \end{bmatrix} \right] \begin{Bmatrix} x_A \\ \theta_A \\ x_B \\ \theta_B \end{Bmatrix} \quad (1)$$



 



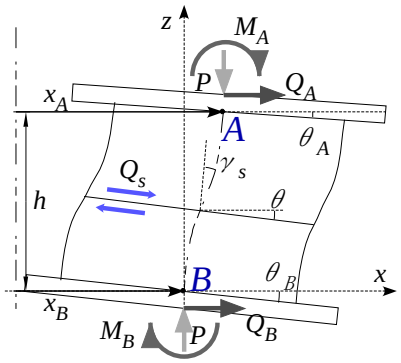


Fig.3 – Deformation of laminated rubber bearing

In Figure 3, $Q_A$ and $Q_B$, $M_A$ and $M_B$, $x_A$ and $x_B$, and $\theta_A$ and $\theta_B$ represent the shear forces, bending moments, horizontal displacements, and bending rotational angles at points *A* and *B*, respectively. *P* represents the axial load acting on the laminated rubber bearing, and *h* represents the total height of the laminated rubber bearing.

The geometric nonlinearity ($P-\Delta$ effect and the influence of the horizontal component of the axial load) can be considered by using the matrix $[K_P]$. $K_h$ represents the horizontal stiffness of the laminated rubber bearing as a function of the axial load on it (Eq.(2)). $P_{cr}$ and $A_e$ represent the axial buckling load and effective plane area of the laminated rubber bearing, respectively. $K_r$ represents the rotational stiffness of the laminated rubber bearing, as a function of the axial load and the horizontal displacement (Eq.(3)). $\phi_{rc}$ represents the dependency of horizontal displacement. $I_e$ represents the effective geometrical moment of inertia of the laminated rubber bearing. Other details are provided in a previous study [4].

$$K_h = K_s\left\{1-\left(\frac{P}{P_{cr}}\right)^2\right\}, \quad \left(K_s = \frac{G\cdot A_e}{n\cdot t_r}\right) \tag{2}$$

$$K_r = K_{rc}\left\{1-\left(\frac{P}{P_{cr}}\right)^2\right\}\cdot \phi_{rc} = K_{rP}\cdot\phi_{rc}, \quad \left(K_{rc} = \frac{E_{rb}\cdot I_e}{n\cdot t_r}\right) \tag{3}$$

## 2.3 The Seismic Wave

The seismic wave used in the dynamic analyses is simulated using a response spectrum on the engineering bedrock of the building standard law in Japan. The level of the response velocity spectrum, $S_v$, is 0.8 m/s when the damping ratio is h = 0.05. This wave is simulated with a random phase. Figure 4 shows the time history and response velocity spectrum of the seismic wave.

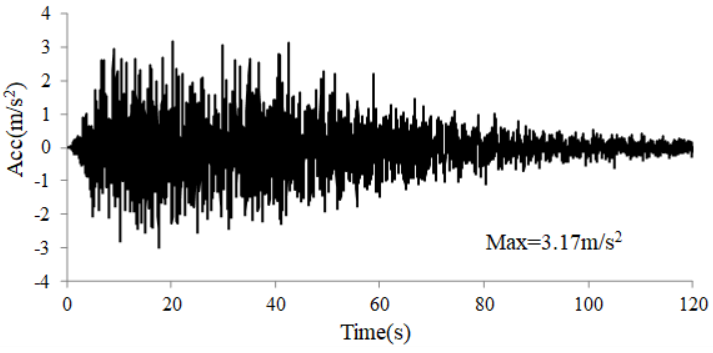


(a) Time history

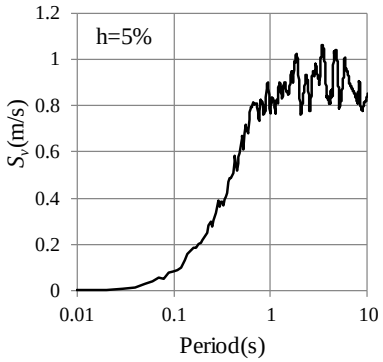


(b) Response velocity spectrum

Fig.4 – Seismic wave



 



## 3. Characteristics of Laminated Rubber Bearing by Dynamic Analyses

### 3.1 Horizontal Stiffness of Laminated Rubber Bearing

Figure 5 shows an example of the hysteresis loop (shear force–horizontal deformation relation) of the laminated rubber bearing located on the outer part X11-line (Figure 1). The horizontal stiffness of the laminated rubber bearing is reduced by the rotation of the bottom part. From Figure 5, the decrease of the horizontal stiffness is large when the horizontal deformation is positive, and the decrease of the horizontal stiffness is small when the horizontal deformation is negative. This is because when the horizontal deformation is in the positive quadrant, the axial force increases, and the pile top rotational angle increases. By contrast, when the horizontal deformation is in the negative quadrant, the axial force decreases, and the pile top rotation angle is suppressed.

The equivalent horizontal stiffness $K_{eq}$ of the laminated rubber bearing is derived from a hysteresis loop using the least squares method, as in a previous report [4]. Figure 6 shows $K_{eq}/K_h$, which is the ratio of the equivalent horizontal stiffness $K_{eq}$ and the horizontal stiffness $K_h$ (Eq.(2)) with no rotational deformation. In this figure, the horizontal axis shows the relative stiffness ratio of the thin foundation girder (FG/1G). As shown in Figure 6, the relationship between $K_{eq}/K_h$ and FG/1G shows the same tendency as reported in a previous study [4].

Figure 7 shows the relationship between rotational stiffness ratios $K_{rP}/K_B$ (a simple indicator that divides the rotational stiffness $K_{rP}$ of the laminated rubber bearing by the rotational stiffness $K_B$ of the substructure [4]) and $K_{eq}/K_h$. In Figure 7, the results for the outer part X11-line are shown with square symbols "□", the results for the inner part X6-line are shown with asterisk symbols "✱", and the results of a previous study [4] are shown with diamond symbols. As shown in Figure 7, the results for the outer part X11-line are in close agreement with the previously reported linear approximation formula with constant axial load. The equivalent horizontal stiffness can be estimated by the proposed evaluation method using the rotational stiffness ratio. In Figure 5, although the influences of variable axial loads are detectable, the average stiffness does not deviate much from the case of a constant axial load.

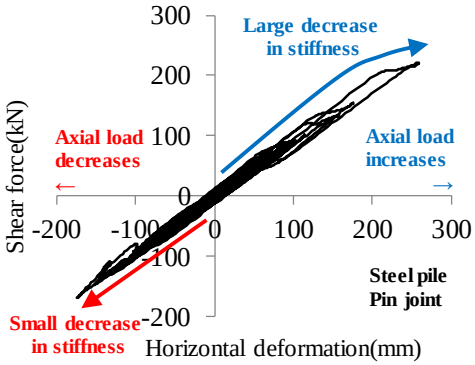


Fig.5 – Hysteresis loop of laminated rubber bearing

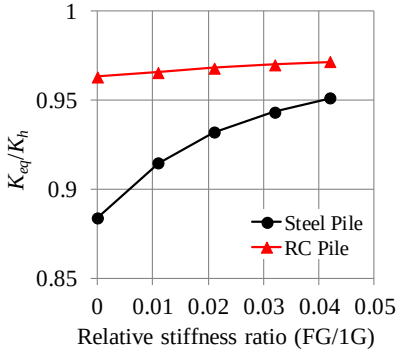


Fig.6 – Relationship of $K_{eq}/K_h$ and relative stiffness ratio (FG/1G)

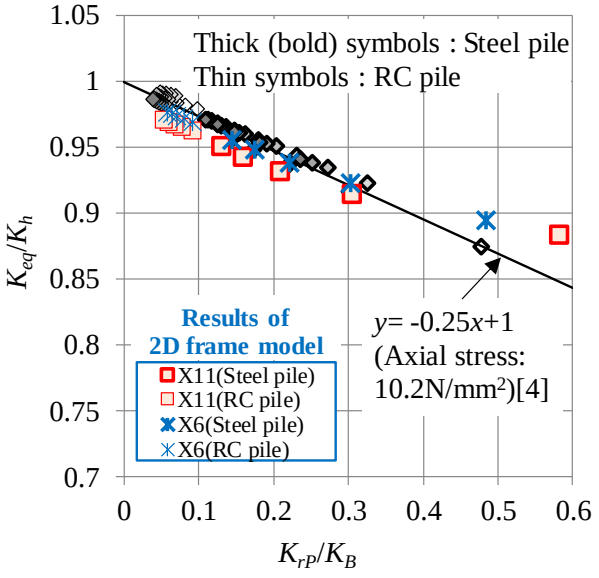


Fig.7 – Relationship of $K_{eq}/K_h$ and $K_{rP}/K_B$



 



### 3.2 Distribution Ratio of the Bending Moment of the Laminated Rubber Bearing

To make a quantitative evaluation of the distribution of the bending moment of the laminated rubber bearing caused by the movement of the inflection point, the ratio of the bending moment $M_A$ of the upper side of the laminated rubber bearing and the bending moment $M_0$ with no rotational deformation is defined as the distribution ratio of bending moment $\alpha_M$ ($=M_A/M_0$) [4].

Figure 8 shows an example of an orbit representing the relationships of distribution ratios of bending moment $\alpha_M(t)$ and the horizontal deformation $\delta(t)$ in the laminated rubber bearing ($t$ : time(s)). In this figure, as $\delta(t)$ increases, $\alpha_M(t)$ converges to a constant value. In the actual structural design, the value of $\alpha_M$ becomes important when the bending moments caused by the $P$–$\Delta$ effect and the shear force of the seismic isolated layer are large. In other words, the value of $\alpha_M$ becomes pronounced only when the horizontal deformation of the laminated rubber bearing is large. Therefore, for $\delta_{\max}$, which represents the maximum horizontal deformation of the laminated rubber bearing, $\alpha_M$ is evaluated by averaging the $\alpha_M(t)$ data when the horizontal deformation of the laminated rubber bearing is more than $0.9 \times \delta_{\max}$.

Figure 9 shows the relationship between $\alpha_M$ and the relative stiffness ratio of the thin foundation girder. The relationship between $\alpha_M$ and FG/1G shows the same tendency as reported in a previous study [4].

Figure 10 shows the relationship between the rotational stiffness ratio $K_{rP}/K_B$ and $\alpha_M$, superimposed on the results reported in a previous study [4]. The square and asterisk symbols represent the results of the X11-line and the X6-line, in the same convention as used in Figure 7, and the other symbols show the results of the previous study [4]. Although the results of the outer part X11-line remain close to the results for the previously reported linear approximation formula with a constant axial load, a slight deviation becomes visible as the value of the rotational stiffness ratio increases. This is because the axial stress of the laminated rubber bearing at $0.9\delta_{\max}$ or more is 12.5–12.8 N/mm$^2$ on average, due to the variable axial load. On the other hand, the results of the X11-line are consistent with the linear approximation formula that was applicable when the axial stress was constant at 12.7 N/mm$^2$, as reported in a previous study [4]. Therefore, $\alpha_M$ of the outer part can be estimated by a linear approximation formula using the maximum value of the variable axial load.

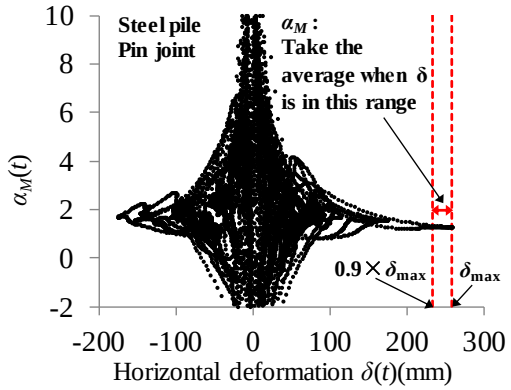


Fig.8 – Relationship of $\alpha_M(t)$ and $\delta(t)$

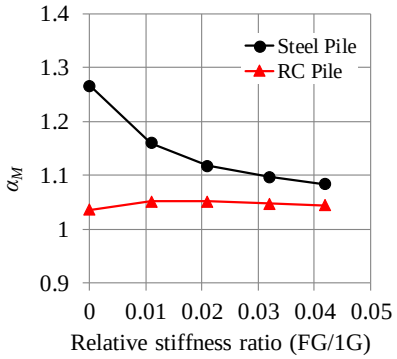


Fig.9 – Relationship of $\alpha_M$ and relative stiffness ratio (FG/1G)

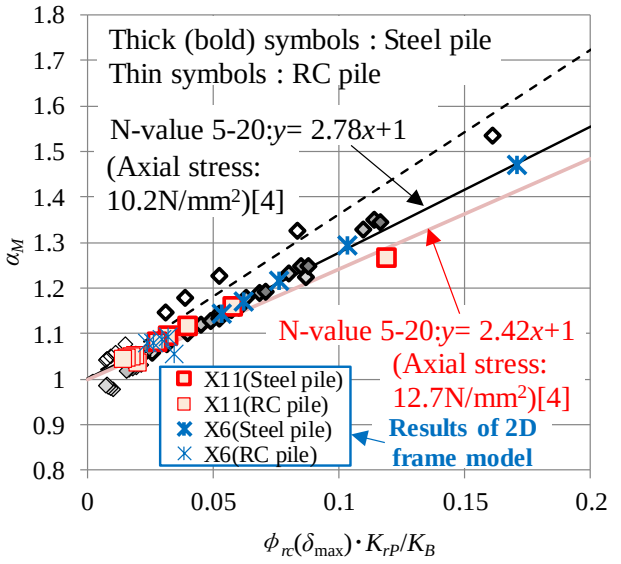


Fig.10 – Relationship of $\alpha_M$ and $\phi_{rc}(\delta_{\max})\cdot K_{rP}/K_B$



 



## 4. The Bending Moment of Piles by Dynamic Analyses

### 4.1 The Maximum Bending Moment Distribution

Figure 11 shows the maximum bending moment distribution of piles located on the X1-line and the X11-line. Absolute values are shown for the bending moment. In this figure, "B" indicates the breadth of the thin foundation girders.

As shown in Figure 11, the maximum bending moment distribution of the X1-line and the X11-line are almost similar, both for steel piles and RC piles. For both types of pile, when the foundation girder is a pin joint, the bending moment is greater at the X11-line (red curves), while the bending moment becomes greater at the X1-line as the breadth of the thin foundation girder increases (black curves). In the case of the pile top seismic isolation system, when the thin foundation girder is a pin joint, the bending moment due to the $P$–$\Delta$ effect acts in the direction in which the pile top moment increases. This is a phenomenon unique to this system.

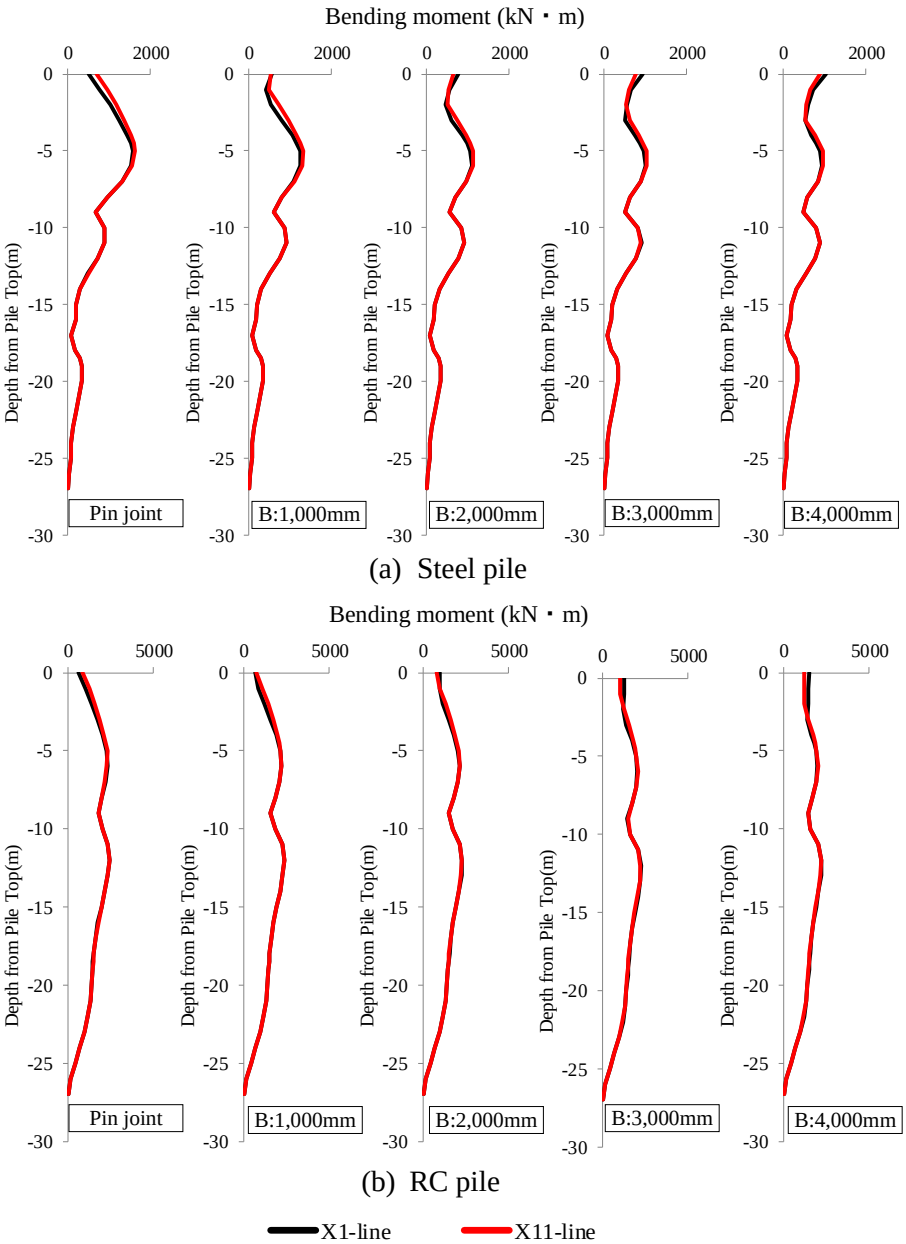


Fig.11 – Maximum bending moment distribution in the outer piles



 



## 4.2 Consideration of Bending Moment of Pile Top

Figure 12(a) shows the bending moment around the pile top located on the X11-line at the time when the inertial force of the superstructure becomes a maximum (t = 45.95 s), for a steel pile with breadth of the foundation girder at 1,000 mm. In this figure, the moment of the pile top is almost zero.

Figure 12(b) shows the bending moment around the pile top at the time when the bending moment of the pile top is a maximum (t = 42.91 s). Figure 13 shows the time history data of the shear forces of the laminated rubber bearing and steel damper, respectively and the acceleration of a point mass located on the foundation girder ("A" in Figure 1). As shown in Figures 12(b) and 13, when the time is t = 42.91 s, the shear force of the laminated rubber bearing is relatively small. Meanwhile, the shear force of the steel damper and the inertial force due to the mass are approximately at their maximum values, which indicates that the bending moment of the pile top has been generated.

As described above, in the pile top seismic isolation system, the bending moment of the pile top may be a maximum when the shear force of the laminated rubber bearing is very small, i.e., when the $P$–$\Delta$ effect is almost zero. This is a peculiar phenomenon in this system and was confirmed in a previous study [5].

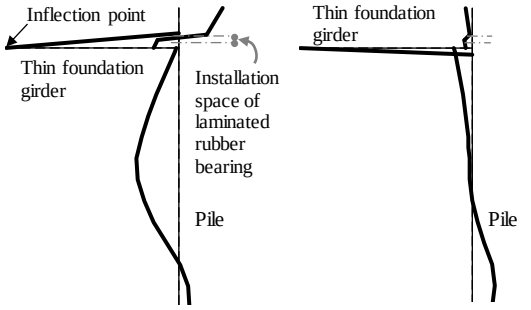


(a) t = 45.95 s (Max. inertial force)  (b) t = 42.91 s (Max. pile top moment)

Fig.12 – Bending moment around pile top (Steel pile, B = 1,000mm)

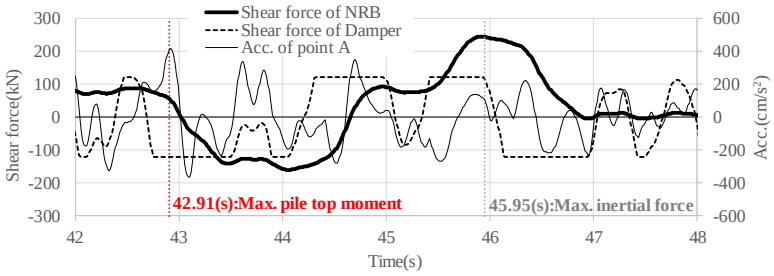


Fig.13 – Time histories of isolation layer shear force and foundation girder's acc.(Steel pile, B = 1,000mm)

## 4.3 Application Method of the Seismic Deformation Method in the Pile Top Seismic Isolation System

In a previous study [5], we proposed an application method of the seismic deformation method for a pile top seismic isolation system. In the present study, we consider the applicability of this method to piles located on the outer part with respect to varying axial loads. The method is outlined in this subsection. In the next subsection, the results shown in subsection 4.1 are compared with those of this method.

Figure 14 shows the analytical models proposed in a previous study [5]. This figure shows the two type states in which the inertial force of the superstructure acts. As described above, in a pile top seismic isolation system, the bending moment of the pile top may reach a maximum when the $P$-$\Delta$ effect is almost zero. Therefore, it is necessary to analyze not only the case where the inertial force is a maximum (Figure 14(a)) but also the case where the $P$–$\Delta$ effect is almost zero (Figure 14(b)), and to consider the bending moment distribution obtained by both analyses.

Figure 14(a) shows the model in which the inertial force is a maximum, considering the distribution ratio of the bending moment $\alpha_M$ described in subsection 3.2. Figure 15 shows the outline of the bending moment distribution at the bottom of the laminated rubber bearing. The equation for calculating $M_0$ is shown in Figure 15. ${}_{iso}Q_{max}$ is the maximum shear force of the seismic isolated layer, and $P$ is the axial load at maximum horizontal deformation.

Figure 16 shows the relationship between the rotational stiffness ratio $K_{rP}/K_B$ and $\alpha_M$, for the laminated rubber bearings located on the X1-line and the X11-line respectively. As shown in Figure 16, the results for the X1-line and the X11-line are consistent with the linear approximation formulas (shown in a previous study [4]) of axial stress 7.6 N/mm$^2$ and 12.7 N/mm$^2$, respectively. In addition, the axial stresses at the time of the



 



maximum inertial force in the dynamic analyses substantially coincide with those axial stresses (7.6 N/mm$^2$ and 12.7 N/mm$^2$). Therefore, in the next subsection, $\alpha_M$ used in this method will be derived by substituting the rotational stiffness ratio $K_{rP}/K_B$ into each linear approximation formula.

Figure 14(b) shows the behavior of the model where the $P$–$\Delta$ effect is almost zero and represents the state shown in Figure 12(b). The yield strength ${}_dQ_y$ of the damper acts on the node located at the center height of the laminated rubber bearing, and the maximum inertial force $W_F \cdot a_{\max}/g$ acts on the node located on a point on the foundation girder (point A). $g$, $W_F$ and $a_{\max}$ are the gravitational acceleration, the weight of the point mass, and the maximum acceleration in the thin foundation girder's point, respectively.

Figure 17 shows the model where the kinematic deformations at the ground (the subsurface layers) have their respective maximum values. As in the conventional method, the maximum ground deformations obtained by the ground dynamic analysis were applied to this model.

The proposed method is based on the seismic deformation method, and it evaluates the maximum bending moment distribution of piles by superpositioning both of the bending moment distributions obtained by the methods of Figures 14 and 17 respectively. In the next subsection, we use two methods, "a square root of sum of squares (SRSS)" and "a simple sum," as a superposition technique for the proposed method.

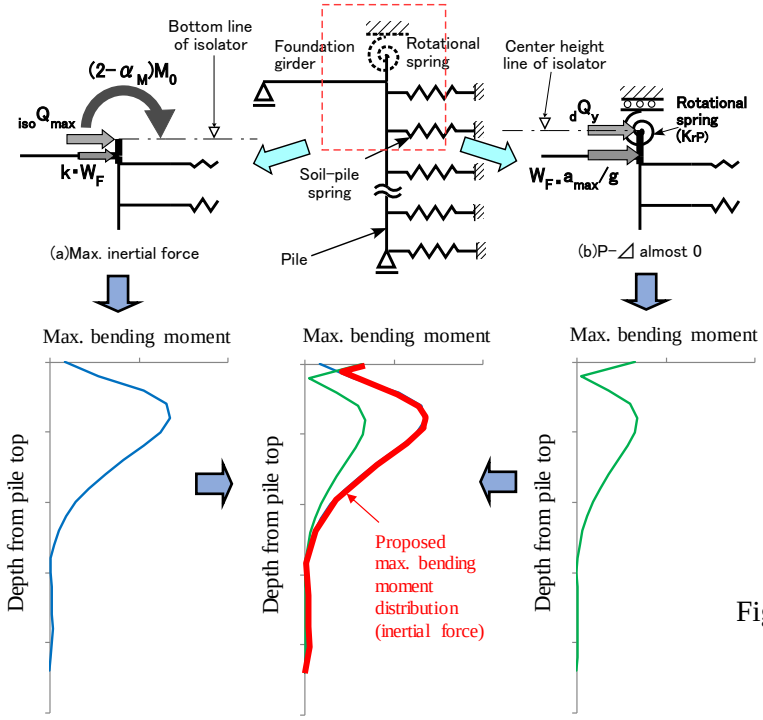


Fig.14 – Analytical models (inertial force) [5]

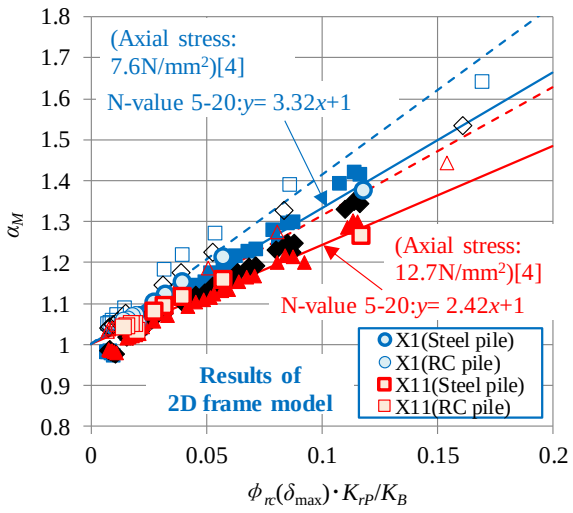


Fig.16 – Relationship of $\alpha_M$ and $\phi_{rc}(\delta_{\max}) \cdot K_{rP} / K_B$ (X1-line and X11-line)

*In Figure 16, the blue squares, triangles and diamonds represent results obtained in a previous study [4].

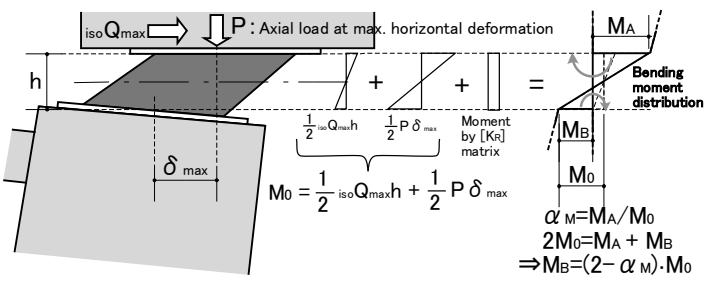


Fig.15 – Relationship of $M_B$ and $\alpha_M$

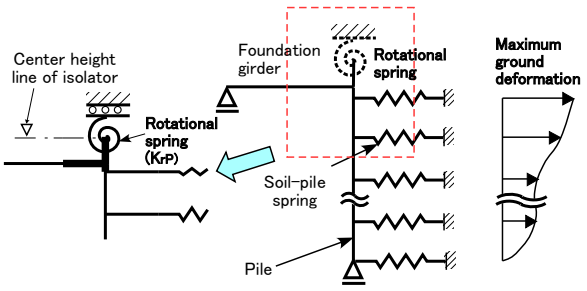


Fig.17 – Analytical model (kinematic) [5]



 



### 4.4 Comparison between Dynamic Analysis and the Proposed Method

Figures 18 and 19 show the maximum bending moment distribution of piles located on the X1-line and the X11-line, respectively and compare the dynamic analysis with the proposed method.

According to the results for steel piles shown in Figures 18(a) and 19(a), evaluation by SRSS of the proposed method shows close agreement of its results with those of dynamic analyses, while the simple sum values are slightly overestimated. The proposed method and the dynamic analyses precisely agree on the values of the bending moment of the pile top.

Meanwhile, according to the results for the RC piles shown in Figures 18(b) and 19(b), evaluation of bending moments by SRSS of the proposed method shows a slight underestimation of values. Additionally, the simple sum closely agrees with the dynamic analyses results. Although the problem in the superposition method of the seismic deformation method, described in a previous study [5], persists, the proposed method can be applied to the outer piles under varying axial loads.

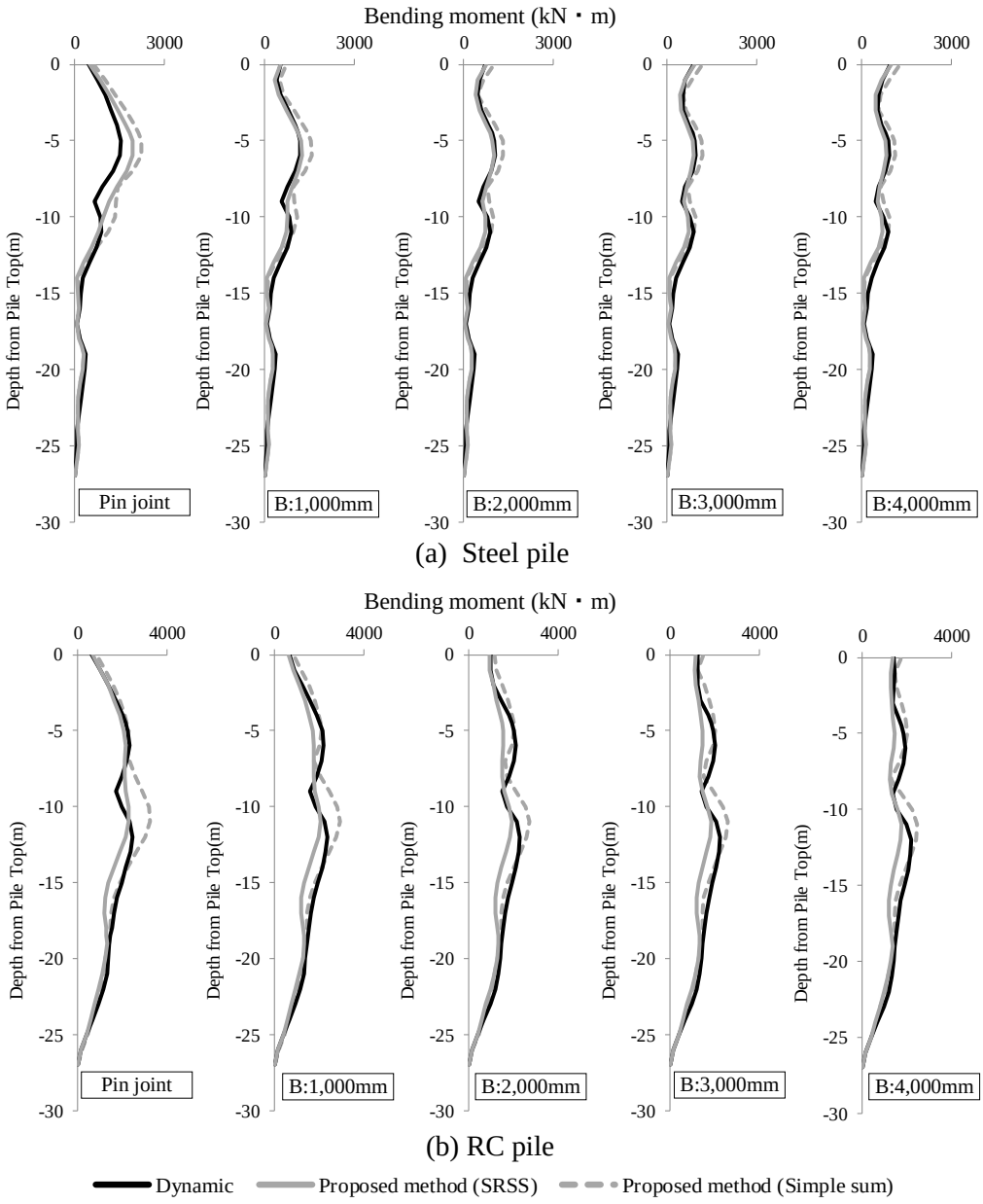


Fig.18 – Maximum bending moment distribution in the outer piles (X1-line)



 



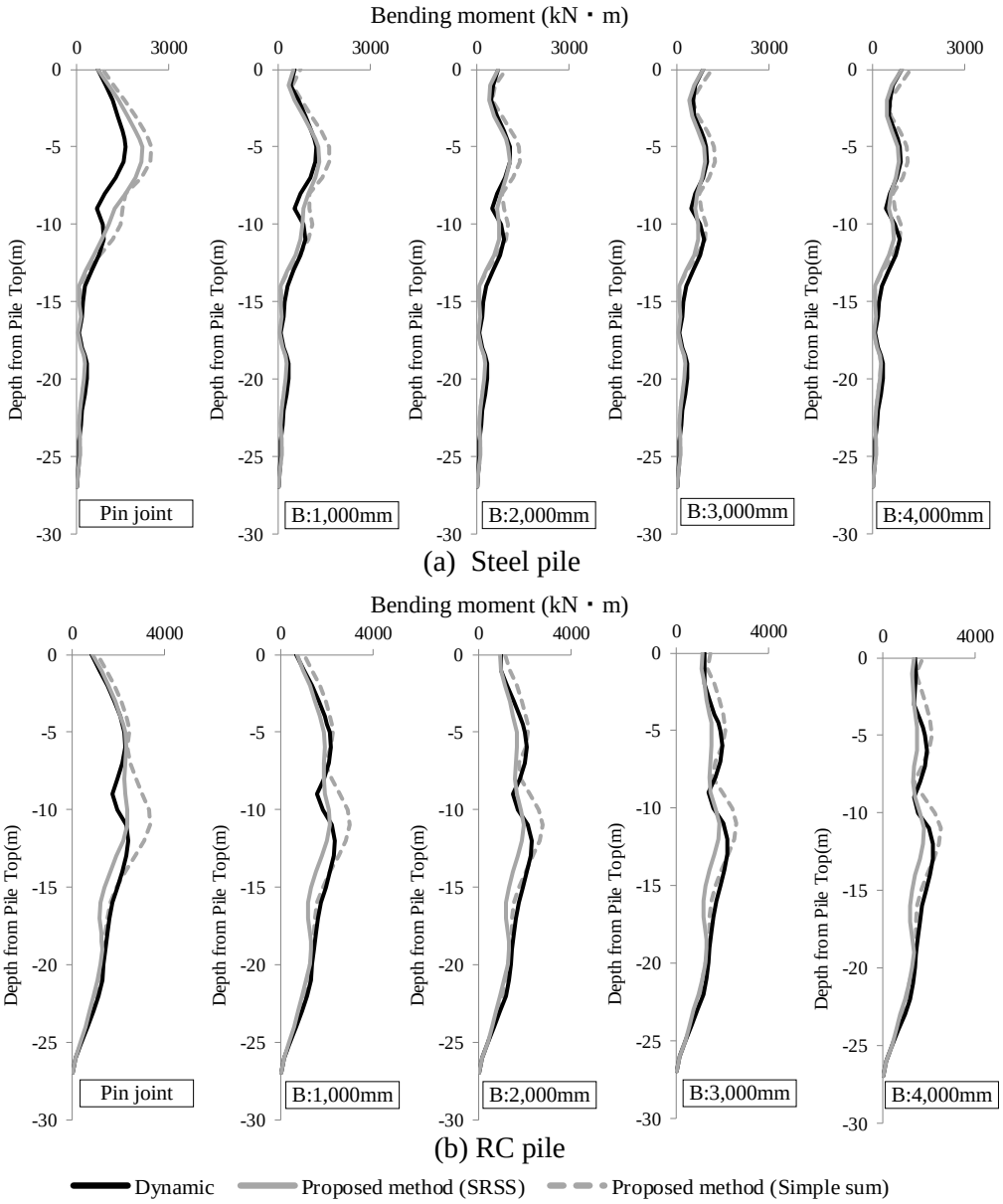


Fig.19 – Maximum bending moment distribution in the outer piles (X11-line)

## 5. Conclusions

In this paper, the dynamic characteristics of laminated rubber bearings and piles located on the outer part of a pile top seismic isolation building were quantitatively evaluated through a set of earthquake response analyses using a two-dimensional frame model.

The following conclusions were drawn.

1) The equivalent horizontal stiffness of a laminated rubber bearing located on the outer part can be evaluated by a previously reported linear approximation formula using the average axial stress acting on the laminated rubber bearing. Meanwhile, the bending moment distribution ratio of a laminated rubber bearing can be evaluated by a linear approximation formula using the peak axial stress acting on the laminated rubber bearing.

2) The bending moment distribution of piles located on the outer part was quantitatively evaluated, and the effects of variable axial loads on the bending moment of the piles, especially on the bending moment of



 



the pile top, were clarified. In addition, the seismic deformation method in a previous paper can be applied to piles located on the outer part by using the bending moment distribution ratios of laminated rubber bearings at the peak axial stress.

## 6. References

[1] M. Kobayashi, S. Shimoda, T. Nishimura (2012): A study on lateral stiffness and design stress of install member on laminated rubber bearings subjected to end rotation. *Journal of Structural and Construction Engineering (Architectural Institute of Japan)*, Vol.77, No.682, 1873-1880, Japan.

[2] T. Miyama (2002): Study on the force-deformation relationships of base-isolation rubber bearing with forced rotation angles at their top and bottom ends. *Journal of Structural and Construction Engineering (Architectural Institute of Japan)*, No.556, 43-50, Japan.

[3] T. Yamauchi, H. Kitamura, M. Nagano, T. Sato, K. Suzuki, Y. Tobita (2016): Study on dynamic characteristics of pile top seismic isolation buildings by earthquake response analysis. *Journal of Structural and Construction Engineering (Architectural Institute of Japan)*, No.730, 2025-2035, Japan.

[4] T. Yamauchi, H. Kitamura, M. Nagano, T. Sato, K. Suzuki (2017): Dynamic characteristics of buildings constructed by pile top seismic isolation system considering nonlinearity of laminated rubber bearing. *16th World Conference on Earthquake Engineering*, Paper No. 1275, Santiago, Chile.

[5] T. Yamauchi, H. Kitamura, M. Nagano, T. Sato, K. Suzuki, Y. Matsuda, Y. Tobita (2018): Study on application of seismic deformation method for pile top seismic isolation buildings. *Journal of Structural and Construction Engineering (Architectural Institute of Japan)*, No.743, 69-79, Japan.

[6] Architectural Institute of Japan (2018): AIJ standard for structural calculation of reinforced concrete structures. Japan.

[7] Architectural Institute of Japan (2019): AIJ standard for allowable stress design of steel structures. Japan.

[8] Architectural Institute of Japan (2006): Seismic response analysis and design of buildings considering dynamic soil-structure interaction. Japan.

[9] K. Ishihara, N. Yoshida, S. Tsujino (1985): Modelling of stress-strain relations of soils in cyclic loading. *Fifth International Conference on Numerical Methods in Geomechanics Nagoya*, 373-380.

[10] K. Koyamada, Y. Miyamoto, K. Miura (2003): Nonlinear property for surface strata from natural soil samples. *38th Japan National Conference on Geotechnical Engineering (The Japanese Geotechnical Society)*, 2077-2078, Japan.

[11] J. A. Haringx (1948, 1949): On highly compressible helical springs and rubber rods and their application for vibration-free mountings I, II, III. *Philips Research Reports*, Vol.3-4.



 